SIAM J. APPL. MATH.
Vol. 60, No. 6, pp. 1997–2008

SINGULARITIES IN DROPLET PINCHING WITH VANISHING VISCOSITY*

JENS EGGERS†

Abstract. A slender-jet model for the pinching of a liquid column is considered in the limit of vanishing viscosity. We find the model to develop a singularity in the gradients of the local radius and the velocity at a finite thread radius, so it does not describe breakup. However, the observed steepening of the profile corresponds to experiments and simulations with fluids at low viscosity. The singularity has a self-similar form, which we compute analytically. The result agrees well with numerical simulations of the model equations.

Key words. capillary breakup, finite-time singularities

AMS subject classifications. 35Q35, 76B45, 35L67

PII. S0036139998334883

1. Introduction. Considerable attention has been devoted recently to the breakup of an axisymmetric column of fluid [1, 2, 3, 4, 5]. The breakup is driven by surface tension forces which reduce the surface area by contracting the fluid thread until its radius goes to zero at a point. Very similar systems have been considered in [6, 7]. As a typical example, we show a drop of water falling from a faucet in Figure 1 [8, 9].

Close to the point of breakup, the interface looks like a cone attached to a nearly flat interface. This is characteristic for low viscosity fluids, where viscosity is important only in a small spatial region around the point of breakup. Details of the initial conditions or external forces like gravity are believed to have little impact on the very localized behavior close to pinch-off. Indeed, experiments with or without gravity and for a variety of nozzle diameters show very similar shapes [4]. This is because surface tension forces become very strong near pinching and drive very small amounts of fluid. Thus the very rapid motion close to breakup is separated dynamically from the motion on the scale of the nozzle diameter both in space and time. A proper measure of length and time are the *local* scales

$$\ell_\nu = (\nu^2\rho)/\gamma, \quad t_\nu = (\nu^3\rho^2)/\gamma^2, \tag{1}$$

which depend only on the properties of the fluid. Here ν is the kinematic viscosity, γ is the surface tension, and ρ is the density of the fluid. In the case that the minimum radius h_{min} of the fluid neck is much smaller than ℓ_ν, a universal pinching solution has been observed [1, 3]. As the radius of the fluid neck goes to zero, surface tension, viscous, and inertial forces are of the same order.

For a low viscosity fluid like water, however, ℓ_ν is only 100 Å, so this asymptotic solution is hardly of relevance experimentally. Accordingly, it would be extremely desirable to develop a similarity theory valid in the range $h_{min} \gg \ell_\nu$. Assuming that all flow features of a hypothetical Navier–Stokes solution are of the same order as h_{min}, it is natural to look at solutions of the inviscid (Euler) equation for that regime.

*Received by the editors March 2, 1998; accepted for publication (in revised form) July 16, 1999; published electronically June 3, 2000. This work was supported by the Deutsche Forschungsgemeinschaft through Sonderforschungsbereich 237.

http://www.siam.org/journals/siap/60-6/33488.html

†Universität Gesamthochschule Essen, Fachbereich Physik, 45117 Essen, Germany (eggers@theophys.uni-essen.de).

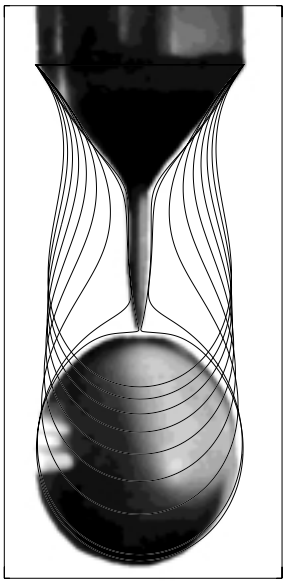

FIG. 1. *A drop of water falling from a faucet* $0.51cm$ *in diameter. The lines represent a computation using one-dimensional model equations. This figure is taken from* [9].

Unfortunately, the Euler equation is known [10] to exhibit spurious blow-up of the local vorticity, even starting from smooth initial data. This problem can be avoided only by considering the subclass of solutions which are irrotational and are thus described by potential flow. Numerical simulations of inviscid, irrotational flow driven by surface tension were used by a number of authors [11, 12] to describe pinching. After the minimum radius has reached a value of about 1/20 of its initial value, all simulations show an *overturning* of the profile. This means that the neck radius $h(z)$ is no longer a single-valued function of the position along the axis z. Recently [5] it was shown that this overturning can be understood as the convergence onto a universal similarity solution of the inviscid, irrotational equations. Similar findings were reported by Chen and Steen [13] for the related problem of a soap film which drives a flow in the surrounding air. Neglecting the inertia of the film, this corresponds to the motion of two fluids of equal density with surface tension between them.

In [14] we use a slender-jet model, originally developed in [9], to address the possible importance of a very small amount of viscosity for pinching in the regime $h_{min} \gg \ell_\nu$. By including the full curvature term the model can quite successfully reproduce experiments in a regime where the profile is not slender [14, 9], although the assumptions going into the formal derivation of the model are violated. As an example, in Figure 1 a few profiles calculated from the model [9] at finite viscosity are superimposed on the experimental picture. In the absence of viscosity this model is often referred to as Lee's model [15]. Using the slender-jet model it is shown [14] that an arbitrarily small amount of viscosity can invalidate scaling arguments based on the inviscid equations alone. This is because of an instability of the inviscid solution which leads to an increase in the gradients of both the local radius and the velocity field like $(t_c - t)^{-1}$. At the singularity time t_c the minimum radius is still finite.

The present paper contains a detailed numerical and analytical study of the singularity of the inviscid equations, which leads to a blow-up of gradients in finite time.

In particular, we construct a local similarity solution which solves the equations for $\nu = 0$. We extend the numerical code used previously in [14] to even smaller viscosities to show that in the limit $\nu \to 0$ of small viscosities the slender-jet equations always select this inviscid singularity. The blow-up occurs while the minimum radius is still finite and an analytical description of the local profiles is given. Thus the inviscid equations are not able to describe breakup, although the full curvature term is kept.

In the next section we introduce the one-dimensional slender-jet model which forms the basis of our analytical description of the inviscid singularity. We then present conclusive numerical evidence for the existence of a inviscid singularity at a time t_c. Derivatives of the surface profile and of the velocity diverge like a power law as function of $t_c - t$. In the third section we present an analytical theory of the inviscid singularity. The resulting surface profiles agree well with numerical simulations.

2. Model and simulations. The main assumption underlying the model of axisymmetric free-surface flow to be considered here is that the fluid motion is directed mostly in the axial direction. This allows us to set up an asymptotic expansion [16] in the thread radius, which at leading order gives equations for the radius $h(z,t)$ of the thread and for the velocity $v(z,t)$, which depend only on the axial coordinate z. In what follows we will deal with the model introduced in [9],

$$\partial_t h = -vh_z - v_z h/2, \tag{2a}$$

$$\partial_t v = -vv_z - p_z + 3Re^{-1}\frac{(h^2 v_z)_z}{h^2}, \tag{2b}$$

$$p = \frac{1}{h(1+h_z^2)^{1/2}} - \frac{h_{zz}}{(1+h_z^2)^{3/2}}, \tag{2c}$$

where the index refers to differentiation with respect to the variable. The fields $h(z,t)$ and $v(z,t)$ have been nondimensionalized using some fixed length scale L of the problem, which in the following is always taken to be the initial radius of the fluid cylinder. The length L can be combined with surface tension γ and density ρ to make up a time scale $T = (\rho L^3/\gamma)^{1/2}$ and a velocity scale $U = L/T$. Every quantity to follow will be nondimensionalized using these units. Combined with the viscosity, it gives the Reynolds number $Re = LU/\nu$.

Equation (2a) expresses mass conservation for a radially uniform velocity field. Conservation of momentum (2b) not surprisingly has the form of Burgers' equation in the inviscid limit, driven by surface tension forces which are proportional to the mean curvature (cf. (2c)). Along the same lines of reasoning (2a)–(2c) were guessed by Lee [15] for $\nu = 0$. By including the full mean curvature in (2c) we have gone beyond the leading-order asymptotics to reproduce exactly the static shape of a hanging drop suspended from an orifice. As an additional benefit, the most dangerous short-wavelength instabilities of the leading-order model $p = 1/h$ [16] have been removed. In fact, the leading-order model is elliptic for $\nu = 0$ [17, 18, 19] and is thus ill-posed as an initial value problem.

In [9, 14] a finite difference scheme was developed capable of simulating (2a)–(2c) at very low viscosities. To resolve the small-scale structures we are interested in, it is crucial to use an adaptive scheme, both in time and space. The minimum thread radius and the maximum gradient of h were taken as predictors where additional spatial resolution was necessary. Thus in a typical run the grid spacing at the position of the inviscid singularity was six orders of magnitude smaller than at the boundary of the computational domain. Since the equations at low viscosity are very sensitive to

noise, grids with smoothly varying grid spacings had to be used, where the spacing did not change by more than 1% from one grid point to the next. With these precautions, no numerical damping or dissipation had to be used, except for the physical viscosity ν. Since the refinement of the grid is only local, the number of grid points needed to achieve a certain resolution Δ only varies like the logarithm of Δ. Thus, starting with $N = 1000$ grid points on the unit interval, a simulation typically ended with $N = 4000$, at which point the resolution had increased by five orders of magnitude.

Since we are interested in the limit of small viscosity, it would be tempting to put $\nu = 0$ directly into (2b). However, we found that as soon as the motion is sufficiently nonlinear, our scheme developed instabilities on the scale of the grid, which caused the code to break down. Thus the inclusion of the full curvature term in (2c) is not enough to stabilize the numerical scheme. Similar short-wavelength instabilities have also been reported in [20] using a finite-element approach. On the other hand, exceedingly small amounts of viscosity are sufficient to stabilize the scheme, even though the viscous term is smaller than the others by several orders of magnitude throughout the domain. In the following, when speaking of a numerical solution of the inviscid equations, we will always refer to the *limit* of zero viscosity at *constant time*.

We also experimented extensively with other means of regularizing the inviscid equations, for example by using numerical viscosities as in [9]. In the upwind differencing scheme introduced in [9], the numerical viscosity is proportional to the grid spacing. The hope was to develop a scheme which automatically converges to the inviscid limit as one increases the resolution. Indeed, if the grid is coarse, a numerical viscosity is often sufficient to remove instabilities. But with improved resolution we always found the instabilities to return. Thus keeping a finite viscosity turns out to be the only reliable and, at the same time, the most physical way of dealing with the instabilities. These results indicate that the system (2a)–(2c) might be an ill-posed initial-value problem, in spite of the short-wavelength regularization introduced by (2c). If on the other hand the problem is well-posed, and the instabilities are a problem of the numerical scheme, the above limit of small viscosity will yield a solution which coincides with the one defined by the inviscid (Lee's) equations.

Figure 2 shows a simulation of (2a)–(2c) at $\mathrm{Re} = 5 \cdot 10^9$ in a liquid bridge geometry with a small sinusoidal perturbation of wavelength $\lambda = 4\pi$ and amplitude $a = 10^{-2}$ superimposed on it. At the ends $z_\pm = 0, 20$ of the computational domain $h(z_\pm, t) = 1$ and $v(z_\pm, t) = 0$ are held constant. Owing to the Rayleigh instability, the bridge starts to pinch. Shown are three profiles close to the inviscid singularity, where the minimum radius has already decreased by a factor of 20. To the right of the minimum, an almost conical neck region is seen; on the other side a round drop has formed. Because of its small radius, the pressure in the flat region is high, pushing fluid over to the right. This causes the interface to perform a sliding motion, which lets the interface become steeper and steeper, since the drop cannot move appreciably owing to its large inertia. Note that the pressure goes to a value close to zero at the eventual place of the inviscid singularity, marked by an arrow.

Next we zoom in on the point around which h_z goes to infinity, marked by an arrow in Figure 2. The value of $\mathrm{Re}^{-1} = 2 \cdot 10^{-10}$ was sufficiently small to resolve the singularity to a maximum slope of $h_z = 10^4$ without viscosity becoming important. This means that the viscous term in (2b) was still three orders of magnitude smaller than all others. An increase of Re^{-1} by a factor of 5 had no significant effect on all simulations to be reported here, implying that all findings are characteristic of the

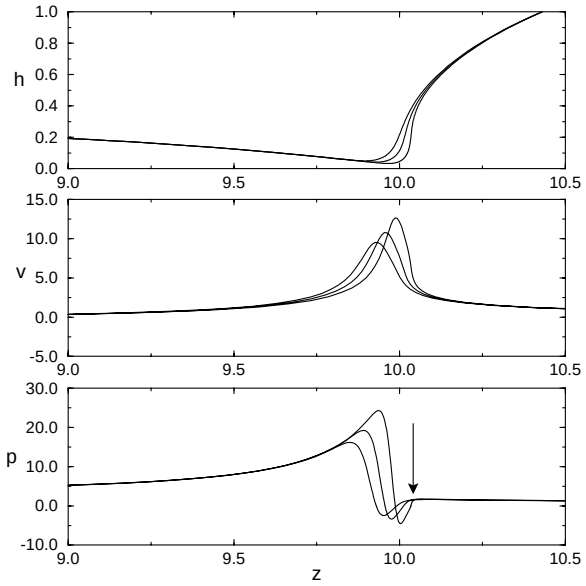

FIG. 2. *A closeup view of simultaneous radius, velocity, and pressure profiles close to the inviscid singularity. The Reynolds number is* $\mathrm{Re} = 5 \cdot 10^9$*, and the time between successive profiles is* $5 \cdot 10^{-5}$*. All profiles are in units of* L *and* T*. The arrow marks the asymptotic location of the shock.*

inviscid limit $\nu \to 0$. With such a small Reynolds number we are no longer able to resolve the huge range of length scales between the outer and the viscous scale, because L/ℓ_ν is now $2 \cdot 10^{19}$. However, the early stages of the evolution of the liquid bridge, where viscous effects are still small, can safely be resolved. In [14] it was demonstrated that the slope goes to infinity near the inviscid singularity and thus the singularity time t_c can be estimated from the blow-up of h_z. It follows from our scaling theory, to be presented in the next section, that $(h_z)_{max} \sim (t_c - t)^{-1}$. Thus t_c can be computed very accurately by plotting $((h_z)_{max})^{-1}$ versus time and fitting with a linear law. In Figure 3 we plot the maximum pressure gradient p_z, which drives the fluid motion, and the maximum velocity gradient as functions of $t_c - t$. It is seen that both p_z and v_z settle on a power law

$$(p_z)_{max} \sim (t_c - t)^{-1}, \quad (v_z)_{max} \sim (t_c - t)^{-1}. \tag{3}$$

The pressure gradient contains the highest (third) derivative in the problem. The fluctuations seen in the curve thus give an estimate of the amount of noise introduced by the regridding procedure. No noise is seen in the first velocity derivative, which clearly confirms the scaling given in (3). We thus see that the inviscid singularity is governed by power law scaling, which will be investigated in more detail in the next section.

We also performed numerous other simulations with different boundary conditions and initial conditions of widely varying amplitude and wavelength. Besides the liquid bridge geometry, where h and v are held fixed at the end of the computational domain, this includes the free boundary problem of [14], which corresponds to a falling drop. In all cases, the same inviscid blow-up (3) was observed, while the minimum jet radius remained finite. This confirms the statement of [9] that Lee's equations do not

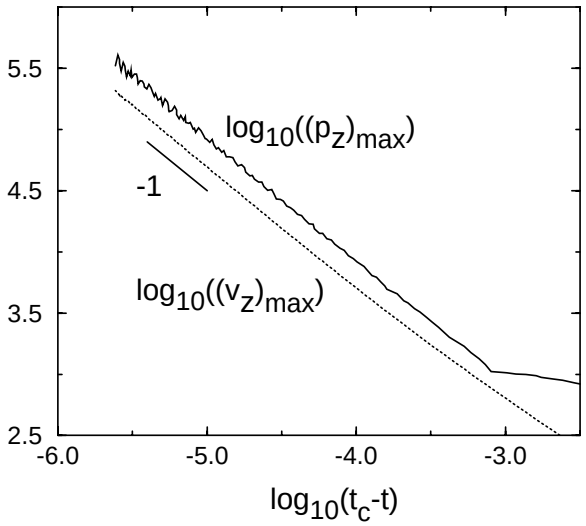

FIG. 3. *The maximum of the gradient of the pressure and of the velocity as function of the time distance from the inviscid singularity. The Reynolds number is* $5 \cdot 10^9$. *Both curves asymptote to a slope very close to* -1.

describe pinching. To further illustrate this point, we have repeated the simulation of Lee's equations reported in [18], with periodic boundary conditions on the interval $[0, 2\pi]$. By using the transformations

$$h(z,t) = S(\epsilon z, \epsilon t), \qquad v(z,t) = W(\epsilon z, \epsilon t) \tag{4}$$

and the initial condition

$$h_0(z) = 1, \quad v_0(z) = -a\sin(\epsilon z), \tag{5}$$

the simulations of section 4.2 in [18] correspond to (2a)–(2c) on the interval $[0, 2\pi/\epsilon]$, the parameter ϵ^2 being 0.1.

On the basis of these simulations it is claimed [18] that h_z goes to infinity at a finite minimum radius for the case $a = 1$, while for a smaller a between 1 and 0.1 a transition to a different type of solution occurs, in which h_z blows up at the same time that the jet pinches, contradicting the results of [9, 14]. Figure 4 shows the profile $h(z)$ for the initial amplitudes $a = 1, 0.1$, and 0.01 at a time when a maximum slope of 10^4 has been reached. Owing to the symmetry of the problem, the computation could be restricted to the interval $[0, \pi/\epsilon]$. The inset shows the minimum height as a function of the maximum slope. The former is seen to asymptote to a constant value of $h_{min} = 0.3$ for $a = 1$ (circles) and $h_{min} = 0.07$ for $a = 0.1$ (squares) and 0.01 (diamonds). The dotted line marks the height of 0.1, where the computations of [18] were stopped due to limited resolution. At that point we find the maximum value of $(h^2)_z$ to be 6.37, in excellent agreement with the reported value [18] of approximately 20ϵ. Since 0.1 lies just above the asymptotic value of h_{min} at small perturbation amplitudes, the limited resolution lead to the erroneous conclusion of a transition to a new type of pinching solution. For initial amplitudes smaller than $a = 0.1$ the solution does not change much, because the initial evolution is in the linear regime, characterized by exponential growth of the prescribed wavelength.

The reason for the observed behavior is that $a = 1$ implies a strong initial flow, which squeezes the liquid cylinder in the middle, steepening the profile. Thus a sufficiently steep front for the shock singularity to set in is produced at a time when the conical solution of Figure 2 is not yet fully developed. For the two smaller amplitudes, on the other hand, the sliding motion of the conical solution described before is responsible for the initial steepening. Thus even if the initial condition does not provoke a steepening, the inviscid dynamics contains a universal mechanism by which sufficiently high slopes are reached eventually. This lends further support to our conjecture that Lee's model does not support pinching.

3. Inviscid similarity solution. We have seen in the previous section that derivatives grow sharply near the inviscid singularity, while on the other hand the height and the velocity remain finite. This means that a similarity ansatz has to include a "background" height and velocity profile, which is slowly varying on the scale of the singular part. At the same time, the singularity may be moving with some speed V_s, which is not necessarily the speed V with which it is convected. Thus one ends up with the similarity form

$$\begin{aligned} h(z',t') &= H + t'^{\alpha} f\left(\frac{z' + V_s t'}{t'^{\beta}}\right), \\ v(z',t') &= V + t'^{\alpha} g\left(\frac{z' + V_s t'}{t'^{\beta}}\right), \end{aligned} \tag{6}$$

where

$$z' = z - z_c \text{ and } t' = t_c - t \tag{7}$$

measure the spatial and the temporal distance from the singularity, respectively. On the spatial scale on which the inviscid singularity develops, H, V, and V_s are approximately constant. Note that (7) has self-similar form, which is superimposed on a traveling wave solution. Also, we assumed $h(z',t')$ and $v(z',t')$ to have the same scaling exponents, because this automatically balances the terms $h_z v$ and $v_z h$ in (2a).

For the ansatz (6) to be consistent, one needs $\alpha > 0$, so in the singular limit $t' \to 0$ one is left with the finite height H and velocity V. For the derivatives to blow up, $\beta > \alpha$. To see whether (6) solves the model equations (2a)–(2c), we balance the most singular terms in t', deriving equations in the similarity variable

$$\eta = \frac{z' + V_s t'}{t'^{\beta}}. \tag{8}$$

One thus finds from (2a)

$$(\beta f' \eta - \alpha f) t'^{\alpha - 1} = -\left[(V - V_s) f' + \frac{1}{2} H g'\right] t'^{\alpha - \beta}. \tag{9}$$

We expect the right-hand side of (9) to make the dominant contribution, which will be the case if $\beta > 1$. This is because then the function f drops out of the equation, and the similarity equations depend only on the derivatives f' and g'. Thus both f and g are determined only up to constants, which are needed for consistency because our ansatz (6) has a free constant built in.

Consequently, the angular bracket must vanish, giving

$$g' = \frac{2(V_s - V)}{H} f', \tag{10}$$

which means that up to constants and a difference in amplitude $2(V_s - V)/H$ the profiles of the height and of the velocity are the same.

Turning to (2b) with $\nu = 0$, one finds to leading order

$$-(V_s - V)g' t'^{\alpha-\beta} = \left(\frac{f''}{f'^3}\right)' t'^{-2\alpha}. \tag{11}$$

Note that the term on the left corresponds to the highest derivatives in p_z as given by (2c). Balancing the left- and the right-hand sides, one finds the scaling law

$$\beta = 3\alpha. \tag{12}$$

Combining (10) and (11), the similarity equation reads

$$-af' = \left(\frac{f''}{f'^3}\right)', \tag{13}$$

where $a = 2(V_s - V)^2/H$. Evidently, the constant a can be eliminated by the transformation

$$\phi(\eta) = a^{-1/3} f'(\eta). \tag{14}$$

The most general solution of the equation for ϕ,

$$-\phi = \left(\frac{\phi'}{\phi^3}\right)', \tag{15}$$

has the form

$$\phi(\eta) = \phi_0 F[\phi_0^{3/2}(\eta - \eta_0)], \tag{16}$$

where $F(\xi)$ is a particular solution of (15).

Equation (13) can easily be solved using standard [21] tricks. In view of the freedom implied by (16), we choose $F(\xi)$ to have its maximum at $\xi = 0$ and to fall off to $1/2$ at $\xi = \pm 1/2$. Then F is given implicitly by

$$\xi = \frac{1}{8F^{3/2}}(1 + 2F)(1 - F)^{1/2}. \tag{17}$$

This function is represented in Figure 5 as the solid line. It decays to zero like $\xi^{-2/3}$ at infinity. In view of the similarity form (6) this ensures that the leading dependence on t' drops out far away from the singular point. This is necessary for the solution to match onto the slowly varying background field.

We note that the singularity described above is not just kinematic in nature, since a contribution from the capillary forcing enters the dominant balance in (11). In addition, the form (6) of the singularity with $V_s \neq V$ implies that it is also a traveling wave. Surprisingly, the local shape (17) of the first derivative of the local radius is identical to that of a local solution $h = H + t' G((z' - Ht')/t'^{3/2})$ of the simple kinematic wave $\partial_t h + h\partial_z h = 0$. (I am grateful to an anonymous referee for this remark.) This can be checked directly from the similarity equation for $G(\xi)$. At present we do not know if this is a coincidence or the result of a deeper analogy.

To test the prediction of the theory, the three profiles of Figure 4, taken at a time when the maximum slope was 10^4, were used for a comparison. In Figure 5

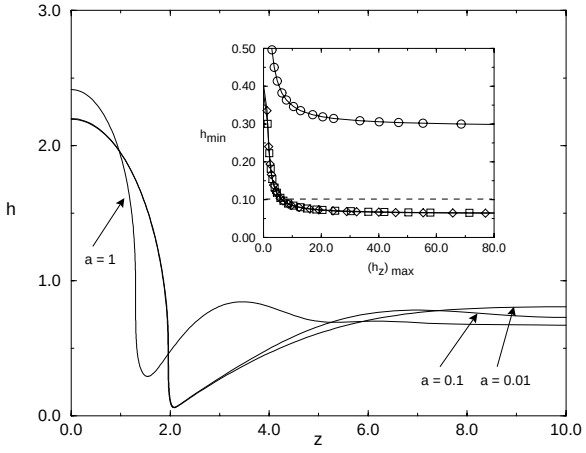

FIG. 4. *A simulation of* (2a)–(2c) *with periodic boundary conditions and initial condition* (5). *The profiles are shown at a time when the maximum slope has reached* 10^4. *The inset shows the minimum radius as a function of the maximum slope for* $a = 1$ *(circles),* $a = 0.1$ *(squares), and* $a = 0.01$ *(diamonds). The dashed line indicates the minimum radius where the simulations* [18] *were stopped.*

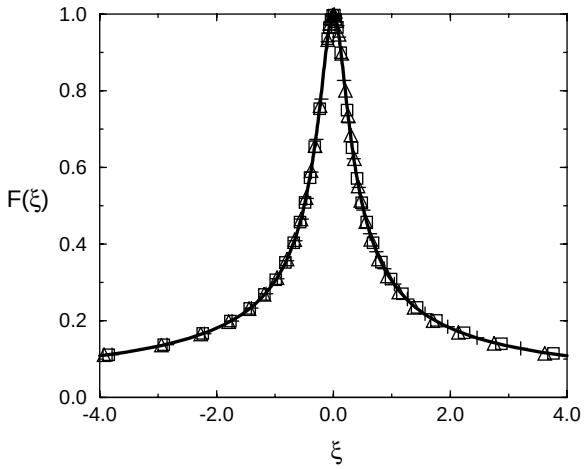

FIG. 5. *The normalized similarity function* $F(\xi)$, *cf.* (14), (16). *The symbols correspond to the simulation of Figure* 4, *for* $a = 1$ *(circles),* $a = 0.1$ *(squares), and* $a = 0.01$ *(diamonds).*

the three profiles of h_z, with the maximum shifted to the origin and the half-width normalized to unity, were superimposed on the theoretical prediction. Although the initial amplitudes were quite different, the local solutions all fall atop of our universal prediction (17). The free constants ϕ_0, η_0 in (16) and the parameter a in (13) are not determined by the similarity theory. Indeed, we confirmed that they depend on initial conditions and therefore cannot come out of a local theory.

Our next concern is to find the scaling exponents α and β, which are not determined from dimensional reasoning as in [1], but which are constrained by the scaling relation (12). In addition, (13) does not depend on the values of the exponents, so α cannot be selected by properties of the similarity equation, as was the case in [22].

To investigate this problem, we must look at next to leading order terms such as the ones contained in (9). Correspondingly, there are subleading terms in h and v which have the form

$$h(z',t') = H + t'^{\alpha} f\left(\frac{z'+V_s t'}{t'^{\beta}}\right) + t'^{2\alpha} f_1\left(\frac{z'+V_s t'}{t'^{\beta}}\right) + \cdots, \tag{18}$$

and correspondingly for $v(z',t')$. Then (2a) becomes at the next to leading order:

$$[3\alpha f'\eta - \alpha f]\, t'^{\alpha-1} = \left[-gf' - \frac{1}{2} f g' + (V_s - V) f_1' - \frac{H}{2} g_1'\right] t'^{-\alpha}. \tag{19}$$

Since the terms must balance, we get

$$\alpha = \frac{1}{2}, \quad \beta = \frac{3}{2}, \tag{20}$$

which are the desired exponents. Note that this conforms with the scaling of both the pressure and the velocity gradient from (3), since

$$p_z \approx t'^{-2\alpha} \left(\frac{f''}{f'^3}\right)' \quad \text{and} \quad v_z \approx t'^{\alpha-\beta} g'. \tag{21}$$

Thus both the value of the exponents and the shape of the profiles is in excellent agreement with theory.

4. Discussion. In [14] we studied the steepening of the height profile for small but finite viscosities. The slopes saturate at a large value, the maximum slope roughly following a scaling law $(h_z)_{max} \sim \mathrm{Re}^{1.25}$. As long as the viscous term is much smaller than the pressure gradient, one can use the inviscid similarity solution. The naive expectation is that the slope saturates as soon as the viscous term is of the same order as the pressure gradient. Using (6) and (20), the temporal scaling of the pressure gradient is $p_z \sim t'^{-1}$ and that of the viscous term $\mathrm{Re}^{-1}(v_z h^2)_z/h^2 \sim \mathrm{Re}^{-1} t'^{-5/2}$, where $\mathrm{Re}^{-1} = \nu/(UL)$ is constant. Equating the two we find $(h_z)_{max} \sim \mathrm{Re}^{2/3}$, which is far too small an exponent. A possible explanation is that the Reynolds numbers for which the exponent 1.25 was found are still too small. But more likely there is an intricate interplay between the inviscid singularity and viscosity, leading to a more complicated intermediate scaling range. Indeed, for the Reynolds numbers considered, the slope continues to grow far beyond the time at which the pressure gradient first balances the viscous term at a point. It thus remains a challenge to find the mechanism which makes the slope saturate.

Equations (2a)–(2c) with ($\nu = 0$) or systems very similar in structure have been used by a number of researchers [15, 23, 24, 25, 20, 26, 17, 18] to describe pinching. However, in Lee's original paper [15] and most of the later work, no attempt is made to resolve the detailed structure of the pinch region. For example, in units of the length of the computational domain, the grid spacing is $dx = 1/20$ in [15] and $1/50$ in [23]. For comparison, the minimum grid spacing used in the present paper is $dx_{min} = 10^{-10}$. In [18] the simulation of (2a)–(2c) with initial conditions (5) was stopped at a minimum radius of 0.1, which for small initial perturbations we showed to be insufficient to find the singularity described here. In [20], which uses a finite element code, the computations were stopped when numerical instabilities on the scale of the grid were observed. The leading-order equations investigated in [26], which use

$p = 1/h$ for the pressure, can also lead to infinite-slope singularities [18]. However, the analytical calculations of [19] show that pinching solutions are also supported for appropriate initial conditions. It remains to be seen whether the inviscid version of the Cosserat model [23], which was also considered in [20], is more well behaved and supports pinching.

We have seen that the slender-jet model (2a)–(2c) in the limit of small viscosity is characterized by more than just the scale of the minimum radius. Instead, a shock-type singularity develops whose width represents another, much smaller scale. This means that inviscid scaling solutions of the type described in [26] become unstable. The crucial question is of course whether a similar mechanism is at work in the small-viscosity limit of the Navier–Stokes equation, which could make this limit singular. It is unlikely that the three-dimensional equation has precisely the same spatial singularity structure as the one found in the model equations, which constrain axial velocity gradients to a far greater extent. Instead it is probable that high-pressure fluid in the neck is injected into the drop, a situation which is only poorly captured by the slice average of the model. The Navier–Stokes equation might thus form a very thin boundary layer around the jet, in which viscosity remains important even for arbitrarily small ν. This is a possible scenario which would invalidate the purely inviscid calculation of [5], at least from a physical point of view.

Even for the model equations, many unanswered questions remain. It is fascinating that even a simple one-dimensional model is capable of such complexity, the key to its understanding lying in the analysis of the singularities.

Acknowledgment. I have benefited greatly from discussions with Michael Brenner.

REFERENCES

[1] J. Eggers, *Universal pinching of 3D axisymmetric free-surface flow*, Phys. Rev. Lett., 71 (1993), pp. 3458–3460.

[2] X. D. Shi, M. P. Brenner, and S. R. Nagel, *A cascade structure in a drop falling from a faucet*, Science, 265 (1994), pp. 219–222.

[3] T. A. Kowalewski, *On the separation of droplets from a liquid jet*, Fluid Dynam. Res., 17 (1996), pp. 121–145.

[4] J. Eggers, *Nonlinear dynamics and breakup of free-surface flows*, Rev. Modern. Phys., 69 (1997), pp. 865–929.

[5] R. F. Day, E. J. Hinch, and J. R. Lister, *Self-similar capillary pinchoff of an inviscid fluid*, Phys. Rev. Lett., 80 (1998), pp. 704–707.

[6] M. C. Pugh and M. J. Shelley, *Singularity formation in models of thin jets with surface tension*, Comm. Pure Appl. Math., 51 (1998), pp. 733–795.

[7] J. Lowengrub and L. Truskinovski, *Quasi-incompressible Cahn-Hilliard fluids and topological transitions*, Proc. Roy. Soc. London A, 454 (1998), pp. 2617–2654.

[8] D. H. Peregrine, G. Shoker, and A. Symon, *The bifurcation of liquid bridges*, J. Fluid Mech., 212 (1990), pp. 25–39.

[9] J. Eggers and T. F. Dupont, *Drop formation in a one-dimensional approximation of the Navier-Stokes equation*, J. Fluid Mech., 262 (1994), pp. 205–221.

[10] R. Grauer, C. Marliani, and K. Germaschewski, *Adaptive mesh refinement for singular solutions of the incompressible Euler equations*, Phys. Rev. Lett., 80 (1998), pp. 4177–4180.

[11] N. N. Mansour and T. S. Lundgren, *Satellite formation in capillary jet breakup*, Phys. Fluids, 2 (1990), pp. 1141–1144.

[12] R. M. S. M. Schulkes, *The evolution and bifurcation of a pendant drop*, J. Fluid Mech., 278 (1994), pp. 83–100.

[13] Y.-J. Chen and P. H. Steen, *Dynamics of inviscid capillary breakup: Collapse and pinch-off of a film bridge*, J. Fluid Mech., 341 (1997), pp. 245–267.

[14] M. P. Brenner, J. Eggers, K. Joseph, S. R. Nagel, and X. D. Shi, *Breakdown of scaling in droplet fission at high Reynolds numbers*, Phys. Fluids, 9 (1997), pp. 1573–1590.

[15] H. C. Lee, *Drop formation in a liquid jet*, IBM J. Res. Develop., 18 (1974), pp. 364–369.
[16] S. E. Bechtel, M. G. Forest, and K. J. Lin, *Closure to all orders in* 1*-D models for slender viscoelastic free jets: An integrated theory for axisymmetric, torsionless flows*, SAACM, 2 (1992), pp. 59–100.
[17] D. T. Papageorgiou, *Analytical description of the breakup of liquid jets*, J. Fluid Mech., 301 (1995), pp. 109–132.
[18] D. T. Papageorgiou and O. Orellana, *Study of cylindrical jet breakup using one-dimensional approximations of the Euler equations*, SIAM J. Appl. Math., 59 (1998), pp. 286–317.
[19] M. A. Fontelos and J. J. L. Velázquez, *On some breakup and singularity formulation mechanisms for inviscid liquid jets*, SIAM J. Appl. Math., 59 (1999), pp. 2274–2300.
[20] R. M. S. M. Schulkes, *Nonlinear dynamics of liquid columns: A comparative study*, Phys. Fluids. A, 5 (1993), pp. 2121–2130.
[21] C. M. Bender and S. A. Orszag, *Advanced Mathematical Methods for Scientists and Engineers*, McGraw-Hill, New York, 1978.
[22] Ch. Uhlig and J. Eggers, *Singularities in cascade models of the Euler equation*, Z. Phys. B, 103 (1997), pp. 69–78.
[23] J. Meseguer, *The breaking of axisymmetric slender liquid bridges*, J. Fluid Mech., 130 (1983), pp. 123–151.
[24] J. Meseguer and A. Sanz, *Numerical and experimental study of the dynamics of axisymmetric slender liquid bridges*, J. Fluid Mech., 153 (1985), pp. 83–101.
[25] R. M. S. M. Schulkes, *Dynamics of liquid jets revisited*, J. Fluid Mech., 250 (1992), pp. 635–650.
[26] L. Ting and J. B. Keller, *Slender jets and thin sheets with surface tension*, SIAM J. Appl. Math., 50 (1990), pp. 1533–1546.